Draft: May 6, 2022
Preprint typeset using LaTeX style AASTeX6 v. 1.0

ALMA IMAGES THE ECCENTRIC HD 53143 DEBRIS DISK

Meredith A. MacGregor[1], Spencer A. Hurt[1], Christopher C. Stark[2], Ward S. Howard[1], Alycia J. Weinberger[3], Bin Ren[4], Glenn Schneider[5], Elodie Choquet[6], Dmitri Mawet[7]

[1]Department of Astrophysical and Planetary Sciences, University of Colorado, 2000 Colorado Avenue, Boulder, CO 80309, USA
[2]Space Telescope Science Institute, 3700 San Martin Dr, Baltimore, MD 21218, USA
[3]Earth & Planets Laboratory, Carnegie Institution for Science, 5241 Broad Branch Road NW, Washington, DC 20015, USA
[4]Observatoire de la Côte d'Azur, Nice, France
[5]Steward Observatory, The University of Arizona, 933 North Cherry Avenue, Tucson, AZ 85721, USA
[6]Aix Marseille Univ, CNRS, CNES, LAM, Marseille, France
[7]California Institute of Technology, 1200 East California Boulevard, Pasadena, CA 91125

ABSTRACT

We present ALMA 1.3 mm observations of the HD 53143 debris disk – the first infrared or millimeter image produced of this ~ 1 Gyr-old solar-analogue. In order to fit models to the millimeter visibilities and constrain the uncertainties on the disk parameters, we adopt an MCMC approach. Previous HST STIS coronagraphic imaging did not detect flux along the minor axis of the disk which was interpreted as resulting from a face-on geometry with two 'clumps' of dust. These ALMA observations reveal a disk with a strikingly different structure. This is the most eccentric debris disk observed to date with a forced eccentricity of 0.21 ± 0.02, nearly twice that of the Fomalhaut debris disk, and shows the same apocenter glow. Although this eccentric model fits the outer debris disk well, there are significant interior residuals remaining that suggest a possible edge-on inner disk, which remains unresolved in these observations. Combined with the observed structure difference between HST and ALMA, these results suggest a potential previous scattering event or dynamical instability in this system. We also note that the stellar flux changes considerably over the course of our observations, suggesting flaring at millimeter wavelengths. Using simultaneous TESS observations, we are able to robustly determine the stellar rotation period of 9.6 ± 0.1 days for the first time.

Keywords: circumstellar matter — stars: individual (HD 53143) — submillimeter: planetary systems

1. INTRODUCTION

While protoplanetary disks are the reservoirs for planet formation, debris disks are the fossil record. Within these remnant disks, asteroids and comets (often referred to as 'planetesimals') collide and grind to continually replenish the population of small dust grains (see review article by Hughes et al. 2018). The presence of debris disks around mature stars is often seen as an indication that earlier planet formation was successful in these systems (e.g., Meshkat et al. 2017). At later evolutionary stages, interior planets now sculpt and stir surrounding disks through gravitational perturbations. Thus, observed structure in debris disks can be traced back to the dynamical influence of planets and used to place constraints on their mass and orbital properties (e.g., Wyatt et al. 1999; Chiang et al. 2009; Hahn & Malhotra 2005; Deller & Maddison 2005, and references therein). Since the dominant exoplanet detection techniques (e.g., transits and radial velocities) are missing analogues to the outer giant planets in our own Solar System (e.g., Zhu & Dong 2021), debris disk structure offers a tantalizing path forward to fill in gaps in the exoplanet census and help put our planetary system into context.

At 18.3 pc (Gaia Collaboration 2020), HD 53143 is a Sun-like (G9V, Torres et al. 2006) star that gives us a glimpse into what a planetary system like our own could have looked like at an earlier stage in its evolution (age ~ 1 Gyr, see discussion in Section 4.4). The outer debris disk was first imaged by Kalas et al. (2006) using ACS on HST, and subsequently imaged by Schneider et al. (2014) using HST STIS. These previous coronagraphic images did not detect flux along the minor axis of the disk which was interpreted as resulting from a face-on geometry with two 'clumps' of dust that could be resonant structures. At longer wavelengths, ISO observations indicated a high fractional luminosity for the system (Moór et al. 2006). Herschel PACS observations at 70 and 160 μm marginally resolved a bright ring

at $\sim 3''$ that appeared elongated to the NW and SE. However, due to Herschel's poor spatial resolution the exact geometry of the disk remained unclear.

In this paper we present the first resolved image of the HD 53143 debris disk at either infrared or millimeter wavelengths made with the Atacama Large Millimeter/submillimeter Array (ALMA). These observations show a striking eccentric disk with features that suggest a previous scattering event or dynamical instability. We discuss the observations and modeling in Section 2 and 3.1, respectively. Section 3.2 presents the modeling results followed by a discussion in Section 4 and conclusions in Section 5.

2. OBSERVATIONS

We used ALMA Band 6 centered at 1.36 mm (238 GHz) to observe the HD 53143 debris disk during Cycle 6. A total of eight scheduling blocks (SBs) were executed between 12–23 March 2019. The details of these observations including the date, number of antennas, shortest and longest baseline lengths, total time on-source, precipitable water vapor (PWV, a measure of the weather quality), and resulting rms noise are provided in Table 1.

The goal of these observations was to resolve the dust structure of the HD 53143 debris disk, so the corrleator was set-up to maximize sensitivity to the millimeter dust continuum emission. Three spectral windows were devoted entirely to continuum emission with a bandwidth of 2 GHz each split into 128 channels and centered at frequencies of 231.5, 244, and 246 GHz. A fourth spectral window with a reduced bandwidth of 1.875 GHz split into 3840 channels was centered on the ^{12}CO J$= 2-1$ line at 230.538 GHz, although no gas emission was detected.

The same calibration sources were used for all eight SBs. Bandpass, flux, and atmospheric calibration along with pointing were performed using the bright blazar J0538-4405 (21.°0 away from the target). Phase calibration made use of J0700-6610. All data processing, calibration, and imaging commands were executed in `CASA` (version 5.4.0, McMullin et al. 2007). Calibrated visibilities produced by the ALMA pipeline were then time-averaged in 30 sec intervals to reduce data volume and improve modeling speed.

3. RESULTS AND ANALYSIS

Our new ALMA image of HD 53143 is shown in Figure 1. This is the first time that the millimeter dust continuum emission has been imaged for this debris disk system. At first glance, the disk is noticeably asymmetric. The bright point source at the image center is coincident with the stellar position, but offset from the disk center. A brightness difference is also apparent between the two 'ansae' (the limb-brightened edges of the disk), with the northwest side farther from the star roughly 3σ brighter than the southeast side closer to the star.

3.1. *Modeling Approach*

In order to quantify the significance of the apparent brightness asymmetry of the HD 53143 disk, we fit both symmetric and eccentric disk models to the ALMA data. We follow the modeling approach first described in MacGregor et al. (2013) and updated for eccentric disks in MacGregor et al. (2017) in order to effectively constrain uncertainties and efficiently explore parameter space. Visibilities are sampled from models of the sky brightness using the `galario` package (Tazzari et al. 2018) and compared directly to the ALMA visibilities within a Markov Chain Monte Carlo (MCMC) framework using the `emcee` package (Foreman-Mackey et al. 2013). For the symmetric model, we assume that the disk is radially symmetric and the surface brightness is described by a power law between an inner radius $R_{\rm in}$ and an outer radius $R_{\rm out}$: $I_\nu \propto r^{-0.5}$, where the power-law index describes the temperature profile and the surface density is assumed to be constant as a function of radius. For the eccentric model, we compute the radial orbital locations of disk particles and create a two-dimensional image by binning using a desired pixel scale. By assuming the same $r^{-0.5}$ temperature profile as for the symmetric model, we can then determine the flux in each pixel. In order to sample the eccentricity parameter space completely and avoid the impact of shot noise as discussed in Kennedy (2020), we use a minimum of 10^7 particles. Both models are normalized to a total flux $F_{\rm disk} = \int I_\nu d\Omega$ and include a point source to describe the detected stellar flux, $F_{\rm star}$, and offsets relative to the pointing position in RA and DEC, $\Delta\alpha$ and $\Delta\delta$, respectively.

We assume uniform priors for all parameters in both models, although some bounds are applied in order to ensure that the models are physical: $F_{\rm disk} > 0$, $F_{\rm star} > 0$, $0 < R_{\rm in} < R_{\rm out}$. To fully explore the parameter space of each model and ensure that all parameters have converged, we use $\sim 10^6$ iterations (100 walkers, 10,000 steps each). We check for convergence by examining all chains and requiring the Gelman-Rubin statistic $\hat{R} < 1.1$ for all model parameters (Gelman & Rubin 1992). The one-dimensional marginalized probability distributions for all model parameters appear Gaussian. For the eccentric model, we do note a degeneracy between the forced (e_f, global orbital shape of the disk) and proper (e_p, intrinsic orbital scatter for individual particles) eccentricity.

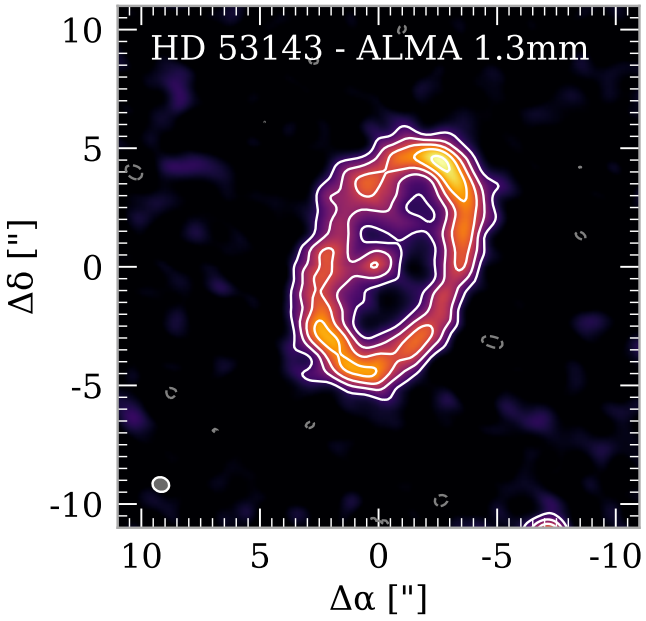

Figure 1. The first millimeter image of HD 53143 taken with ALMA shows an asymmetric distribution of dust with a bright point source in the center coincident with the star. Contours are in steps of 3σ ($3\times$ the rms noise of 5.6 μJy beam^{-1}). The gray ellipse in the lower left corner indicates the $1\farcs13 \times 0\farcs92$ synthesized beam with natural weighting.

3.2. *Modeling Results*

Table 2 presents the best-fit model parameters for both the symmetric and eccentric models. The symmetric model is unable to reproduce the data without significant stellar offsets, which makes it clear that an eccentric model is required to describe the HD 53143 debris disk. Figure 2 shows the ALMA 1.3 mm data (left panel) along with the best-fit symmetric and eccentric models (top and bottom, respectively) displayed at full resolution (left center) and imaged like the ALMA data (right center). The residuals resulting from subtracting the best-fit model from the data are shown at right. It is clear 'by eye' that the eccentric model does a much better job fitting the structure of the outer debris disk. The symmetric models leaves $> 3\sigma$ residuals on the apocenter (northwest) side of the disk. This conclusion is supported by the reduced χ^2 values of X and X for the eccentric and symmetric models, respectively. However, both models leave $> 6\sigma$ residuals interior to the outer disk. These significant residuals are clear evidence that there is additional structure in this system that we are currently failing to resolve with our observations.

4. DISCUSSION

We have presented the first millimeter image of the HD 53143 debris disk. This new ALMA image shows that the disk is clearly eccentric exhibiting the same apocenter glow seen previously in the Fomalhaut debris disk. Here, we discuss the eccentricity of the disk, a potential inner disk, and the dynamical implications of these results. In addition, we compare the structure of disk as observed by ALMA and HST and consider apparent variability in the star's emission during the course of our observations that could be due to flaring.

4.1. *Eccentric Structure*

HD 53143 is the most eccentric debris disk observed to date ($e_f = 0.21 \pm 0.02$) and the second example of a disk in which we have detected apocenter glow. Since bodies on Keplerian orbits move more slowly at apocenter than pericenter, theory predicts that we should see a surface density enhancement at this location in the disk (Pan et al. 2016). At shorter infrared wavelengths, where emission is optically thick, grain temperature dominates producing a brightness enhancement at pericenter closer to the star. At longer millimeter wavelengths, where emission is optically thin, observations are more sensitive to surface density and apocenter glow can be seen. The first conclusive detection of this effect was made using ALMA observations of the Fomalhaut debris disk ($e_f = 0.12 \pm 0.01$, MacGregor et al. 2017). These new observations of HD 534143 show that this effect can be expected in any eccentric debris disk.

Unlike Fomalhaut, which has a proper eccentricity of $e_p = 0.06 \pm 0.04$, the best-fit for the HD 53143 disk is almost twice as high with $e_p = 0.11 \pm 0.01$. In general, low e_p indicates that particles are on apsidally aligned orbits resulting in

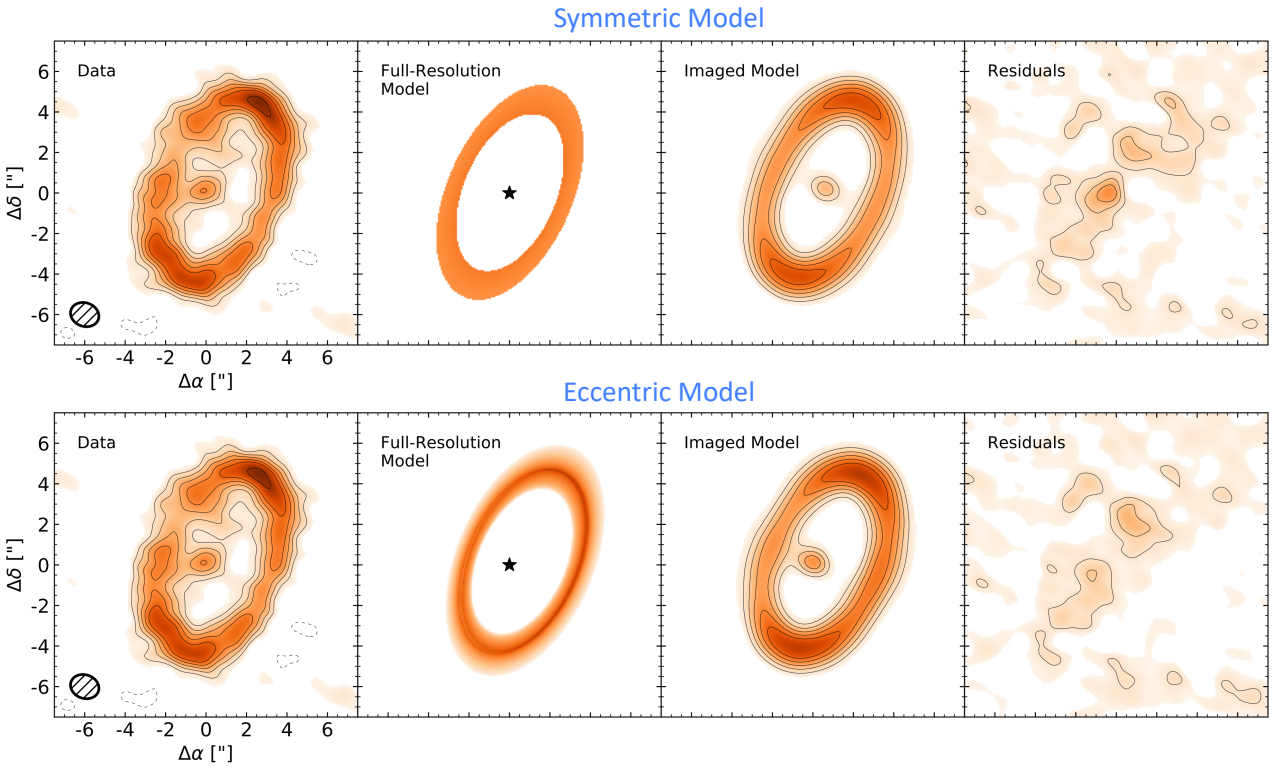

Figure 2. An eccentric disk model *(top)* provides a better fit to the ALMA data than a symmetric one *(bottom)*. In both figures, panels are as follows: *(left)* the ALMA 1.3 mm continuum image, *(left, center)* the best-fit model at full resolution, *(right, center)* the best-fit model imaged like the data with no noise, and *(right)* the residuals produced by subtracting the best-fit model from the data. Contours are in steps of 3σ ($3\times$ the rms noise of 5.6 μJy beam^{-1}) in all panels. As in Figure 1, the gray ellipse in the lower left corner indicates the $1\farcs13 \times 0\farcs92$ synthesized beam with natural weighting.

a disk that is narrower at pericenter than at apocenter. The width of an eccentric disk is influenced by two parameters: the range of semi-major axes of bodies orbiting within the disk, Δa, and the proper or intrinsic eccentricity of those bodies' orbits, e_p. Depending on which of these dynamical parameters dominates, theory predicts that we should observe azimuthal variations in the disk width, with the largest difference between apocenter and pericenter.

If the disk is sculpted through secular perturbations of a planet, we expect Δa to dominate. In this case, the elliptical orbits of bodies in the disk are the same shape but of differing sizes. The expected width ratio between pericenter and apocenter depends on the magnitude of the proper eccentricity, e_p, compared to the forced eccentricity imparted by a perturbing planet, e_f. If the proper eccentricity is much smaller than the forced eccentricity ($e_p < e_f$), the ratio of the widths at pericenter to apocenter is expected to be $1 - e_f : 1 + e_f$, i.e., the width will be narrower at pericenter than at apocenter. If instead, the proper eccentricity is comparable to the forced eccentricity ($e_p \sim e_f$), the width ratio should be closer to unity.

A more extreme ratio of widths is possible if e_p dominates. Dermott & Murray (1980) propose a combination of self-gravitation, particle collisions, and close-packing to produce an extreme 'pinching' of a belt at pericenter. The ϵ ring of Uranus has a width of ~ 20 km at pericenter compared to ~ 96 km at apocenter, implying a width ratio of $\sim 1:5$ (Elliot & Nicholson 1984). At the same time, higher values of e_p can result in a disk with uniform width around its entire circumference. Within the resolution limits of the current ALMA data, the disk width does indeed appear to be fairly uniform as a function of azimuthal angle. This result does, however, imply that a simple planetary sculpting scenario might be less likely. Combined with the presence of a potentially misaligned inner disk (see Section 4.2 below), a previous scattering event or dynamical instability may be required.

4.2. *Inner Dust Emission?*

Given the significant excess of millimeter emission interior to the outer debris ring, it is clear that there is a source of dust in the inner part of the HD 53143 system. The two 6σ peaks on either side of the star are suggestive of limb brightening from an edge-on inner disk. If we assume this interpretation, we can constrain the potential radius and

width of this inner ring to be $\sim$ 25 AU (1.″4) and $\sim$ 5 AU (0.″3), respectively, given the separation of the two peaks, with a maximum flux density of $\sim$ 80 μJy. Since the current ALMA observations only achieve a resolution of roughly 20 AU, this inner disk would not be well-resolved. Earlier HST observations also indicated the presence of an inner ring, but with very different geometry – extending from 5 – 55 AU (0.″3 – 3.″1) and face-on (i.e., inclination of 0°, Schneider et al. 2014). Interestingly, both of these inclinations (face-on or edge-on) would imply that the inner and outer rings are not aligned. In order to explain such a large misalignment, a significant scattering event, potentially involving migration of giant planets, must have happened earlier in the system's history.

Another possibility is that dust from the outer ring is being passed inwards. The η Corvi system includes a hot inner dust ring and a cold outer belt that has been previously resolved by ALMA. In order to replenish the inner disk, material must flow from the outer to the inner disk. Marino et al. (2017) suggest that a stable planetary system could scatter material and feed a close-in collisional cascade. Another option is that grains could be scattered inwards by a planet and then transported through Poynting-Robertson drag. Future observations with higher spatial resolution are required to definitively show us what mechanism or structure is responsible for the observed inner excess emission in the HD 53143 system, and as a result reveal the dynamical history of this planetary system.

4.3. *Comparison to Scattered Light Observations*

Previous HST coronagraphic imaging suggested that the HD 53143 disk might be face-on with resonant clumps of emission. New HST STIS observations (Ren et al., in prep.) show that this is not the case and that the disk is in fact inclined relative to the line of sight. However, while the ALMA data is best fit by a thin ($h < 0.04$) disk, the HST data require a significant scale height of $h \sim 0.3$. Unlike every other detected inclined debris disk, the HD 53143 disk shows no forward-scattering side at visible wavelengths. In fact, it shows the opposite – an absence of flux near the minor axes and an enhancement of flux near the ansae. The only way to produce this is via a semi-inclined disk with large scale height, or a disk viewed edge-on. ALMA observations trace thermal emission from roughly millimeter-sized grains. HST observations trace scattered light from small, micron-sized grains. Thus, the difference in scale height between these two observations suggests that the dynamics of large vs. small grains are different in the HD 53143 disk. One possible explanation is that the small grains are getting stirred and puffed up by a giant planet orbiting within the disk (e.g., Quillen & Faber 2006; Pan & Schlichting 2012).

4.4. *Stellar Emission*

The ALMA observations of HD 53143 were executed over eight nights in March 2019. Although the sensitivity is not high enough to split the data up further, we are able to fit the flux of the star in each of these eight observations separately. The results are shown in Fig 3. Assuming that HD 53143 is a G9V star, the expected photospheric flux at 1.3 mm is just 33 μJy. In observations 2 and 5–8, the best-fit flux for the star is significantly in excess of this value. The excess is most extreme in observation 6, when the star is $> 3\times$ brighter than we would expect in quiescence. This transient behavior on roughly hour-long timescales is consistent with stellar flaring, which has now been observed from several M dwarf stars (MacGregor et al. 2018, 2020).

Serendipitously, the Transiting Exoplanet Survey Satellite (TESS) observed HD 53143 simultaneously with our ALMA observations (light curve is shown in gray in Figure 3). Although no significant flares are apparent, the periodic variations in brightness are indicative of spot modulation. We expect that millimeter emission is similar to FUV in that it traces particle acceleration in flares, while TESS traces the resulting photospheric heating (MacGregor et al. 2020). It is notable that stars observed to flare in the FUV (and therefore presumably in the millimeter) sometimes have no flares in the TESS bandpass (Loyd et al. 2020). Similarly, Williams et al. (2014) suggest that radio-loud dwarfs may be explained by constant low-level particle acceleration without producing heating in other bands. Because of its extreme southern declination, HD 53143 is actually near the continuous viewing zone for TESS and was observed in 14 additional sectors. We use a Lomb-Scargle periodogram to determine the rotation period for the star to be 9.6 ± 0.1 days. The rotation-age relation for a G9/K0 dwarf in Curtis et al. (2019) gives 10 days as the expected rotation period at 1 Gyr, although some K0 dwarfs with 10 day periods are as young as 670 Myr.

5. CONCLUSIONS

In this paper, we present the first ALMA image of the HD 53143 debris disk. This disk had only been imaged previously in scattered light with HST coronagraphic observations. Our ALMA observations yield new insights on the structure of this young solar analogue, revealing a clearly eccentric disk that displays apocenter glow. In order to constrain the geometry of the disk, we adopt an MCMC framework to fit models directly to the millimeter visibilities. Our main conclusions are as follows:

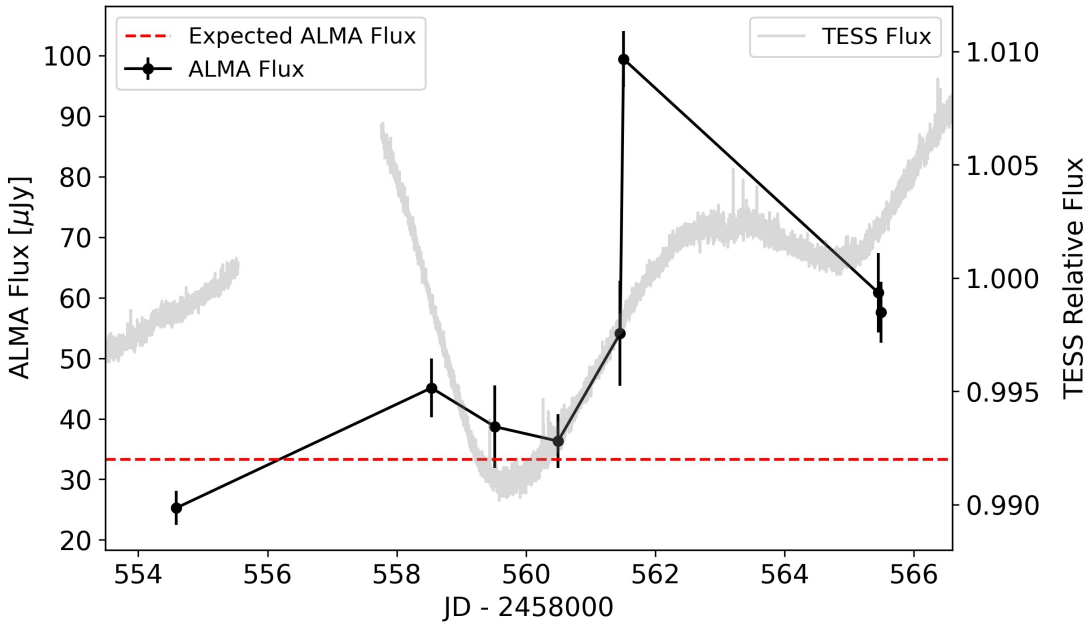

Figure 3. The flux density of the central star varies over the course of our eight ALMA observations, indicating potential flaring. Each point in this light curve represents the best-fit stellar flux density in each individual observation. For reference, the expected photospheric flux of 33 μJy for a G9V star is indicated by the dashed red line. Simultaneous TESS observations plotted in gray indicate significant spot modulation.

1. The best-fit model constrains the disk eccentricity to be 0.21 ± 0.02, considerably higher than the Fomalhaut debris disk. In addition, the proper eccentricity of the disk is 0.11 ± 0.01, much higher than the Fomalhaut disk. This result suggests that orbits in the disk are not apsidally aligned.

2. Although this eccentric model reproduces the outer disk structure well, $> 6\sigma$ residuals remain interior. These could be due to an additional inner disk or dust from the outer ring being passed inwards.

3. Modeling of HST and ALMA observations does not produce consistent results for the structure and geometry of the outer disk. Since HST observations trace micron-sized grains and ALMA observations trace millimeter-sized grains, this suggests that small and large grains are experiencing different sculpting mechanisms.

4. The stellar flux varies considerably over the course of our observations, with a clear peak in observation 6. We interpret this as evidence for millimeter flaring. Simultaneous TESS observations suggest considerable spot modulation. Using the complete TESS light curve, we have made the first determination of the rotation period for this star of 9.6 ± 0.1 days.

The HD 53143 debris disk is an intriguing system that may have undergone a previous scattering event or dynamical instability. Its unique characteristics certainly suggest a need for future study as a test bed to consider the effects of planetary migration on debris disk structure. ALMA observations with higher resolution would be able to resolve an inner disk if present and look for any variation in the disk width as a function of azimuthal angle. With this critical information, we would be able to place strong constraints on the orbits and masses of any planets in the system.

This paper makes use of the following ALMA data: ADS/JAO.ALMA #2018.1.00461.S. ALMA is a partnership of ESO (representing its member states), NSF (USA) and NINS (Japan), together with NRC (Canada) and NSC and ASIAA (Taiwan) and KASI (Republic of Korea), in cooperation with the Republic of Chile. The Joint ALMA Observatory is operated by ESO, AUI/NRAO and NAOJ. The National Radio Astronomy Observatory is a facility of the National Science Foundation operated under cooperative agreement by Associated Universities, Inc.

M.A.M. acknowledges support for part of this research from the National Aeronautics and Space Administration (NASA) under award number 19-ICAR19_2-0041.

Software: `CASA` (v5.4.0 McMullin et al. 2007), `galario` (Tazzari et al. 2018), `emcee` (Foreman-Mackey et al. 2013), `Lightkurve` (Lightkurve Collaboration et al. 2018), `astropy` (Astropy Collaboration et al. 2013, 2018), `astroquery` (Ginsburg et al. 2019)

REFERENCES

Astropy Collaboration, Robitaille, T. P., Tollerud, E. J., et al. 2013, A&A, 558, A33

Astropy Collaboration, Price-Whelan, A. M., SipHocz, B. M., et al. 2018, aj, 156, 123

Chiang, E., Kite, E., Kalas, P., Graham, J. R., & Clampin, M. 2009, ApJ, 693, 734

Curtis, J. L., Agüeros, M. A., Douglas, S. T., & Meibom, S. 2019, ApJ, 879, 49

Deller, A. T., & Maddison, S. T. 2005, ApJ, 625, 398

Dermott, S. F., & Murray, C. D. 1980, Icarus, 43, 338

Elliot, J. L., & Nicholson, P. D. 1984, in IAU Colloq. 75: Planetary Rings, ed. R. Greenberg & A. Brahic, 25–72

Foreman-Mackey, D., Hogg, D. W., Lang, D., & Goodman, J. 2013, PASP, 125, 306

Gaia Collaboration. 2020, VizieR Online Data Catalog, I/350

Gelman, A., & Rubin, D. B. 1992, Statistical Science, 7, 457

Ginsburg, A., Sipőcz, B. M., Brasseur, C. E., et al. 2019, AJ, 157, 98

Hahn, J. M., & Malhotra, R. 2005, AJ, 130, 2392

Hughes, A. M., Duchêne, G., & Matthews, B. C. 2018, ARA&A, 56, 541

Kalas, P., Graham, J. R., Clampin, M. C., & Fitzgerald, M. P. 2006, ApJL, 637, L57

Kennedy, G. M. 2020, Royal Society Open Science, 7, 200063

Lightkurve Collaboration, Cardoso, J. V. d. M., Hedges, C., et al. 2018, Lightkurve: Kepler and TESS time series analysis in Python, Astrophysics Source Code Library, ascl:1812.013

Loyd, R. O. P., Shkolnik, E. L., France, K., Wood, B. E., & Youngblood, A. 2020, Research Notes of the AAS, 4, 119

MacGregor, M. A., Osten, R. A., & Hughes, A. M. 2020, arXiv e-prints, arXiv:2001.10546

MacGregor, M. A., Weinberger, A. J., Wilner, D. J., Kowalski, A. F., & Cranmer, S. R. 2018, ApJL, 855, L2

MacGregor, M. A., Wilner, D. J., Rosenfeld, K. A., et al. 2013, ApJL, 762, L21

MacGregor, M. A., Matrà, L., Kalas, P., et al. 2017, ApJ, 842, 8

Marino, S., Wyatt, M. C., Panić, O., et al. 2017, MNRAS, 465, 2595

McMullin, J. P., Waters, B., Schiebel, D., Young, W., & Golap, K. 2007, in Astronomical Society of the Pacific Conference Series, Vol. 376, Astronomical Data Analysis Software and Systems XVI, ed. R. A. Shaw, F. Hill, & D. J. Bell, 127

Meshkat, T., Mawet, D., Bryan, M. L., et al. 2017, AJ, 154, 245

Moór, A., Ábrahám, P., Derekas, A., et al. 2006, ApJ, 644, 525

Pan, M., Nesvold, E. R., & Kuchner, M. J. 2016, ApJ, 832, 81

Pan, M., & Schlichting, H. E. 2012, ApJ, 747, 113

Quillen, A. C., & Faber, P. 2006, MNRAS, 373, 1245

Schneider, G., Grady, C. A., Hines, D. C., et al. 2014, AJ, 148, 59

Tazzari, M., Beaujean, F., & Testi, L. 2018, MNRAS, 476, 4527

Torres, C. A. O., Quast, G. R., da Silva, L., et al. 2006, A&A, 460, 695

Williams, P. K. G., Cook, B. A., & Berger, E. 2014, ApJ, 785, 9

Wyatt, M. C., Dermott, S. F., Telesco, C. M., et al. 1999, ApJ, 527, 918

Zhu, W., & Dong, S. 2021, ARA&A, 59, arXiv:2103.02127

Table 1. 2019 ALMA Observations of HD 53143

Obs. ID	Date	Time Range (UTC)	# of Ants.	Baseline Lengths (m)	On-Source Time (min)	PWV (mm)	rms (mJy)
1	12 March	02:07:13.4 – 03:04:03.2	46	14–360	49.63	1.29	14.6
2	16 March	00:50:56.3 – 01:47:22.4	47	14–360	49.67	1.26	15.0
3	17 March	00:27:33.3 – 01:24:01.0	47	14–360	49.62	1.74	16.7
4	17–18 March	23:53:09.7 – 00:49:31.6	44	14–313	49.62	2.17	18.6
5	18 March	22:56:23.5 – 23:53:00.0	45	14–313	49.63	3.08	20.8
6	19 March	00:13:01.4 – 01:09:37.4	45	14–313	49.62	2.64	19.9
7	22 March	22:45:10.1 – 23:41:39.2	47	14–360	49.65	2.18	16.3
8	22–23 March	23:53:32.8 – 00:50:00.5	46	14–360	49.63	2.11	16.7

Table 2. Best-Fit Model Parameters

	Parameter	Description	Symmetric Model	Eccentric Model
Disk Geometry	a	Disk radial position [au]	88.3 ± 0.9	90.1 ± 0.5
	Δa	Disk width [au]	29.7 ± 1.0	19.7 ± 2.5
	h	Disk scale height	0.04 ± 0.02	0.04 ± 0.02
	i	Inclination [deg]	56.1 ± 0.4	56.2 ± 0.4
	PA	Position angle [deg]	156.4 ± 0.4	157.3 ± 0.3
	ω_f	Argument of pericenter [deg]	–	112.8 ± 2.1
Flux	$F_{\rm tot}$	Total disk flux [mJy]	1.36 ± 0.03	1.42 ± 0.03
	$F_{\rm star}$	Total stellar flux [mJy]	0.05 ± 0.01	0.05 ± 0.01
Eccentricity	e_f	Forced eccentricity	–	0.21 ± 0.02
	e_p	Proper eccentricity	–	0.11 ± 0.01
Offset	$\Delta\alpha$	RA offset [″]	-0.60 ± 0.01	0.07 ± 0.06
	$\Delta\delta$	DEC offset [″]	0.17 ± 0.02	0.04 ± 0.04